IEEE Photonics Journal
An IEEE Photonics Society Publication

Open Access

Hadamard Matrix Design for a Low-Cost Indoor Positioning System in Visible Light Communication

Volume 9, Number 2, April 2017

Jong Kang Park, ***Member, IEEE***
Tae-Gyoo Woo
Myoungha Kim
Jong Tae Kim, ***Member, IEEE***

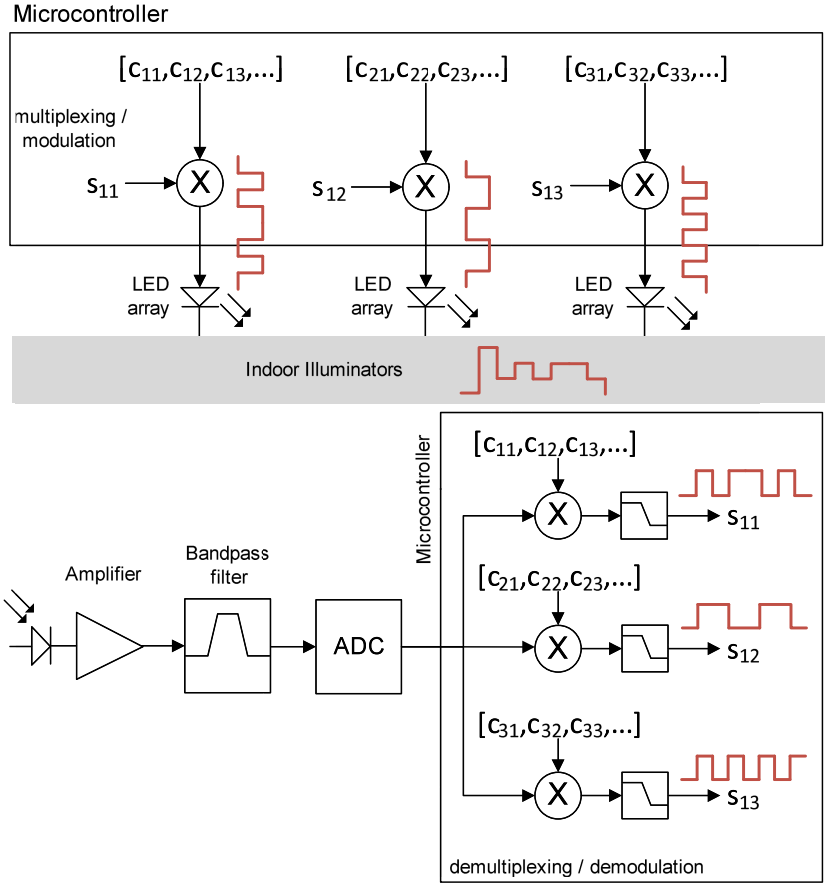

DOI: 10.1109/JPHOT.2017.2667038
1943-0655 © 2017 IEEE

IEEE photonics SOCIETY

IEEE

Hadamard Matrix Design for a Low-Cost Indoor Positioning System in Visible Light Communication

Jong Kang Park, *Member, IEEE*, Tae-Gyoo Woo, Myoungha Kim, and Jong Tae Kim, *Member, IEEE*

School of Electronic and Electrical Engineering, Sungkyunkwan University, Suwon 440-746, South Korea

DOI:10.1109/JPHOT.2017.2667038

Manuscript received August 1, 2016; revised February 1, 2017; accepted February 6, 2017. Date of publication February 9, 2017; date of current version March 1, 2017. This work was supported by the Basic Science Research Program through the National Research Foundation of Korea funded by the Ministry of Education (2015R1D1A1A01061304). Corresponding author: J. T. Kim (e-mail: jtkim@skku.edu).

Abstract: A positioning system based on visible light communication (VLC) utilizes illuminating indoor lights to identify the location of objects. The complexity and the cost of VLC are largely affected by limited bandwidths on optical emitters and detectors. In this paper, we present an optical signaling and multiplexing technique, which employs Hadamard matrices to implement a multiple-input multiple-output (MIMO) system. Fundamental conditions to create nonnegative optical signals and brightness control are defined in conjunction with multiplexing different sources and receiving messages. By using two design methods $n-1$ and M constructions, Hadamard matrices can be used to implement MIMO VLC without considering bandwidth limits for emitters or receivers. Eventually, the presented model and the method generalize multiplexing techniques with orthogonality from a view of orthogonal matrices. Experiments show that the proposed positioning system has 0.02-m standard errors of identification due to the noise component in a slow optical receiver.

Index Terms: Visible light communication (VLC), indoor positioning, indoor localization, light emitting diode (LED), photodetector, Hadamard matrix, orthogonal code.

1. Introduction

Visible light communication (VLC) provides optical signaling by illuminating light emitting diodes (LEDs) easily dispatched throughout our daily life. The indoor positioning system is the one of the derivative applications of VLC, as a competitor or a hybrid component for the existing heterogeneous sensor technologies [1]. Due to its availability and the cost as an illuminator, it is highly competitive in data communication and sensing systems for various indoor applications. Replacing with LEDs, laser diodes (LDs) are also being considered for expanding the capacity and speed of high-end VLC systems [2], [3].

Intensity modulation and direct detection (IM/DD) of the optical power and the carrier has been used to indoor localization in VLC [4], [5]. Several studies have proposed methods of identifying locations of moving terminals using VLC [6]. The signal-to-noise ratio (SNR) is one of key metrics determining not only data rates and the capacity of the optical channel but the exact object location as the optical sensing system as well. Multiple optical sources and receivers implement multiple

input multiple output (MIMO) systems to increase the capacities and data rates of optical channels [4], [5], [7]. As in typical wireless communication, optical orthogonal frequency division multiplexing (OFDM) with real and positive signaling has been employed as a modulation technique for multiple LEDs to enhance the spectral efficiency [5], [8]–[10]. Additionally, an extensive study for indoor MIMO-OFDM has been reported involving a multi-user support [5]. However, the bandwidth of light signaling in LEDs is typically limited to 20–50 MHz with separate red-green-blue emitters and up to 2 MHz in a blue emitter combined with a yellow phosphor [7], [11]. Low-cost off-the-shelf photodiode and amplifier modules are not readily capable of sensing with more than tens of MHz of acquisition rate [12]. Therefore, if the cost, complexity and applicability are taken into account for a VLC infrastructure including receivers, application of FDM with a variety of optical frequencies for individual LED units can be difficult.

To overcome this limitation, a few optical code division multiple access (CDMA) techniques [11], [13], [14] have been applied to VLC. As in optical OFDM, the signals should be unipolar and nonnegative during transmission. Without perfect orthogonality in the applied codes, the cross-correlation properties for concurrent transmission signals is degraded in such systems [11], [13]. In [14], a mapping process from bipolar to unipolar signals and *vice versa* was presented to ensure the cross-correlation property. However, it is difficult to extract the received bipolar symbol unless the number of affected transmitters is correctly identified prior to de-multiplexing at the receiver. Moreover, acquired signal levels at the receiver are more important than the mapped symbols for positioning system to exactly estimate the distances between the sources and the receiver.

This paper focuses on Hadamard matrices and their variants that can be used in VLC positioning system with low complexity and low cost. A single carrier or non-carrier frequency can be employed to load transmitted signals from each emitter. The code sequence is directly interpreted as on-off keying (OOK) optical signals. Separated signals are spread by the specific row or the column of Hadamard codes and then decoded by the same code at the receiving end. This approach was originally motivated by capacitive touch sensors [15] where the bandwidth of the carrier frequency is tightly constrained by panel structures and materials. In VLC positioning, a few optical carrier frequencies can also be chosen in order to avoid external noise sources. Then, the signal-to-interference-and-noise ratio (SINR) of the optical signal becomes mainly dependent on the cross-correlation property of the given orthogonal codes which can be naturally addressed by their inherent orthogonal property. This paper also suggests a condition satisfying perfect orthogonality that can be used to develop another code or multiplexing methods for VLC MIMO. Brightness controls and elimination of the ambient light are naturally implemented by the presented properties.

2. System Design

We first employ an optical MIMO system model that consists of N_t transmitters and N_r receivers [4]. Considering IM/DD of $N_r \times N_t$ bipolar data matrix $\boldsymbol{s}$ where $s_{ij} \in \{-1, 1\}$, the transmitted signal matrix $\boldsymbol{x}$ and received data matrix $\boldsymbol{y}$ are defined as

$$\boldsymbol{x} = \alpha_t \cdot (\beta_{drv} \cdot \boldsymbol{C}_r \cdot \boldsymbol{s} \cdot \boldsymbol{C}_t + \boldsymbol{b}_t) \tag{1}$$

$$\boldsymbol{y} = \beta_{rcv} \cdot \left\{\alpha_r \cdot \boldsymbol{C}_r^{\top} \cdot (\boldsymbol{x} \circ \boldsymbol{H}) \cdot \boldsymbol{C}_t^{\top} + \boldsymbol{n}\right\} \tag{2}$$

$$\text{s.t. } N_{ct} \geq N_t,\ N_{cr} \geq N_r,\ \boldsymbol{C}_t\boldsymbol{C}_t^{\top} = N_{ct} \cdot \boldsymbol{I}_{N_t},\ \boldsymbol{C}_r^{\top}\boldsymbol{C}_r = N_{cr} \cdot \boldsymbol{I}_{N_r}$$

where $\boldsymbol{C}_t$ and $\boldsymbol{C}_r$ having -1 or 1 elements are $N_t \times N_{ct}$ and $N_{cr} \times N_r$ orthogonal matrices for both optical emitters and receivers, respectively. N_{ct} and N_{cr} are the numbers of spreading codes in transmitters and receivers, respectively. $\boldsymbol{I}_n$ denotes an $n \times n$ identity matrix where the diagonal elements are all ones. Identities for $\boldsymbol{C}_t\boldsymbol{C}_t^{\top}$ and $\boldsymbol{C}_r\boldsymbol{C}_r^{\top}$ define the orthogonality of the Hadamard matrices. Modulating and multiplexing the concurrent symbol $\boldsymbol{s}$ are achieved by multiplication with $\boldsymbol{C}_t$ in (1). Similarly, de-modulating and de-coding a received signal vector will be performed by $\boldsymbol{C}_r$ in (2). Each spread code in N_{ct}-length or N_{cr}-length sequence can be expanded to time-domain samples where full waveform for modulation is represented. In that case, each element in $\boldsymbol{C}_t$ or $\boldsymbol{C}_r$

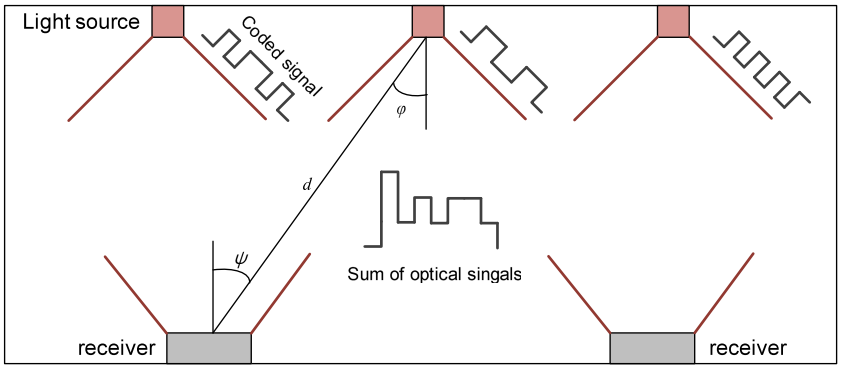

Fig. 1. Multiple transmitters and receivers configuration in indoor VLC.

is a real number and range from [−1, 1]. During transmissions, by adding the bias $\boldsymbol{b}_t$ in $N_{cr} \times N_{ct}$ and by using the scaling factor β_{drv} to switch −1 and 1 data at LEDs, all elements of x are corrected as real and non-negative numbers. Brightness control required in IEEE 802.15.7 [16] can also be provided by the use of $\boldsymbol{b}_t$. Appropriate orthogonal codes, $\boldsymbol{C}_t$ and $\boldsymbol{C}_r$ to support (1) and (2) will be further explained in Section 3. The constant α_t and α_r are conversion parameters for electric signal to optical signal and *vice versa*. Compared to β_{drv}, β_{rcv} is an operational gain at the receiver circuitry. It can be represented by a gain or a conversion ratio for the amplifier stage. The term $\boldsymbol{x} \circ \boldsymbol{H}$ in (2) produces the matrix whose elements are $x_{ji} \cdot h_{ji}$ by the element-wise product $\circ$. $\boldsymbol{H}$ denotes an $N_r \times N_t$ channel matrix where each channel gain h_{ji} obeys an optical propagation model [5], [16]–[18] from emitter i to receiver j along a directed line-of-sight (LOS) with d_{ji} distance

$$h_{ji} = \begin{cases} \frac{(m+1)A_j}{2\pi d_{ji}^2} \cdot \cos^m(\phi)\cos(\psi), & 0 \geq \psi \geq \Psi_{1/2} \\ 0, & \text{elsewhere} \end{cases} \tag{3}$$

Φ and Ψ are transmitter and receiver semi-angles as depicted in Fig. 1. In (3), $m = -\ln 2 / \ln(\cos \Phi_{1/2})$. For a Lambertian transmitter, we set $\Phi_{1/2}$ to 60°, but for a directed emitter, $\Phi_{1/2} = 15°$ [17]. At a bare detector, $\Psi_{1/2}$ is also approximated as $\pi/2$, but by adding a concentrating structure to a bare detector, it can be less than $\pi/2$ as in [4]. A_j means the physical area of the photodetector (PD) in receiver j. In this paper, we also assume that there is no reflection, diffraction and refraction of the visible lights. Only LOS links are available at the receiving ends. In (1), an element of noise matrix $\boldsymbol{n}$ comprises the real valued additive white Gaussian noise (AWGN) component with mean μ_{amb} and variance σ_{ji}^2. Shot noise, thermal noise and other components model each element of $\boldsymbol{n}$ as in [4]. More detailed models including received optical power and pre-amplifier noise current were introduced in [17]. In this paper, we primarily employ thermal and shot noise components with normal distribution, but these components are collectively added in (2) during the reception of excited optical signals. Even if the thermal noise is still driven by the light source drivers, this approach is simple and more convenient, because the entire noise component $\boldsymbol{n}$ with μ_{amb} includes in-band ambient light noise levels after the demodulation stage and the remaining thermal components appear as aggregated noise levels at the receiver circuitry. If $\alpha_t \cdot \alpha_r \simeq 1$ in (1) and (2), assuming the ideal conversion of optical and electrical signals, the SINRs of individual y_{ji} for i-to-j link can be derived as

$$\text{SINR}(y_{ji}) = \frac{h_{ji} \cdot \beta_{drv} \cdot E_s \cdot N_{ct} \cdot N_{cr}}{\sigma_{ji}^2} \tag{4}$$

where E_s is the energy for transmitting a unit signal $\in \{-1, 1\}$. Note that β_{rcv} is not included in (4). Both noise and acquired signal levels are proportional to β_{rcv}. Assuming that β_{rcv} and β_{drv} are adjusted to avoid saturation of the maximum operational limits for the source and the receiver, we

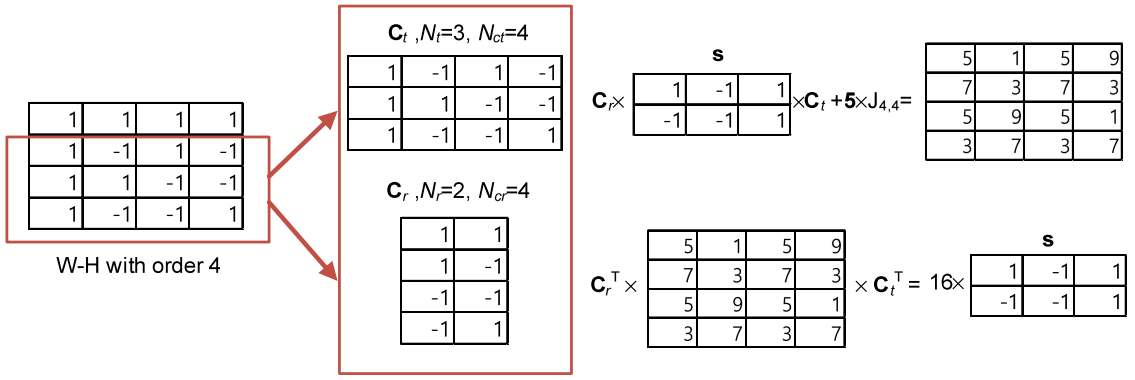

Fig. 2. Biased orthogonal matrix design derived from the normalized Hadamard matrix.

can define SINR at a single receiver as follows:

$$\text{SINR}\left(y_j\right) = \frac{N_t \cdot h_{ji} \cdot \beta_{drv} \cdot E_s \cdot N_{ct} \cdot N_{cr}}{\sum_i^{N_t} \sigma_{ji}^2} \simeq \frac{\sqrt{N_t} \cdot h_j \cdot \beta_{drv} \cdot E_s \cdot N_{ct} \cdot N_{cr}}{\sigma_{ji}^2} \tag{5}$$

where N_t Gaussian random noise variables with variance σ_{ji}^2 are added. By the rule for addition of independent random variables [19], if σ_{ji} values for all N_t transmitters are the same, SINR will be increased by the square root of N_t times.

3. Hadamard Matrix Design for VLC Positioning

For $\boldsymbol{H}$ in (2), note that there are no different path delays defined during optical propagation along LOS from multiple transmitters to multiple receivers. Delays due to d_{ji}/c are neglected in indoor VLC. N_{ct} and N_{cr} might embed one or more chip periods for the given system. Only considering spreading and de-spreading operations performed by $\boldsymbol{C}_r$ and $\boldsymbol{C}_t$ in (1) and (2), the required orthogonal matrices must have the following equality to ensure zero cross-correlation property in no path delays

$$\boldsymbol{C}_t^{\top} \cdot \boldsymbol{b}_t \cdot \boldsymbol{C}_t^{\top} = \boldsymbol{C}_r^{\top} \cdot (\boldsymbol{b}_t \circ \boldsymbol{J}_{N_{cr},N_{ct}}) \cdot \boldsymbol{C}_t^{\top} = 0 \tag{6}$$

where $\boldsymbol{J}_{n,m}$ means an $n \times m$ matrix of ones. Since both $\boldsymbol{C}_r$ and $\boldsymbol{C}_t$ have non-zero elements, either of the following two conditions should be satisfied to remove the effects of $\boldsymbol{b}_t$ from (6)

$$\boldsymbol{C}_r^{\top} \cdot (\boldsymbol{b}_t \circ \boldsymbol{J}_{N_{cr},N_{ct}}) = 0 \tag{7}$$

where $\boldsymbol{b}_t = \{\boldsymbol{b}_{t,1}, \boldsymbol{b}_{t,2}, \ldots\}$ and $\boldsymbol{b}_{t,j}$ is a column vector with the same N_{ct} elements

$$(\boldsymbol{b}_t \circ \boldsymbol{J}_{N_{cr},N_{ct}}) \cdot \boldsymbol{C}_t^{\top} = 0 \tag{8}$$

where $\boldsymbol{b}_t = \{\boldsymbol{b}_{1,t}, \boldsymbol{b}_{2,t}, \ldots\}$, and $\boldsymbol{b}_{i,t}$ is a row vector with the same N_{cr} elements.

This indicates that any orthogonal matrices for $\boldsymbol{C}_r$ and $\boldsymbol{C}_t$ with all ones can support optical modulation and multiplexing with the existence of bias $\boldsymbol{b}_t$. In this way, $\boldsymbol{b}_t$ can vary for every set of code sequence transmissions and also contributes to the brightness controls. As shown in (4), it is not relevant to SINR. As one of the simplest design, the existing Walsh-Hadamard (*W-H*) matrix [15], [20] in 2^k order can satisfy (7) and (8) by removing the first rows or the first column with all ones. For example, Fig. 2 shows examples of $\boldsymbol{C}_t$ and $\boldsymbol{C}_r$ derived by *W-H* matrix with an order of 4 when $N_t = 3$ and $N_r = 2$. For simplicity, we use $\beta_{drv} = \beta_{rcv} = 1$ and $\boldsymbol{H} = \boldsymbol{J}_{N_r,N_t}$ in (1) and (2). The bias $\boldsymbol{b}_t$ is added after multiplying $\boldsymbol{C}_t$ and $\boldsymbol{C}_r$ to make non-negative x. In any case, when either of (7) or (8) is met, the acquired signal in y is equivalent to the square root of the denominator in (4), regardless of the presence of constant values in a row or in a column of $\boldsymbol{b}_t$. Setting these same constant values gives a background brightness visible to human eyes while the rate of the optical signal change is greater than 200 Hz [12], [16]. In Fig. 2, all elements of $\boldsymbol{b}_{3,t}$ are set to 5 to increase the average value of optical signals.

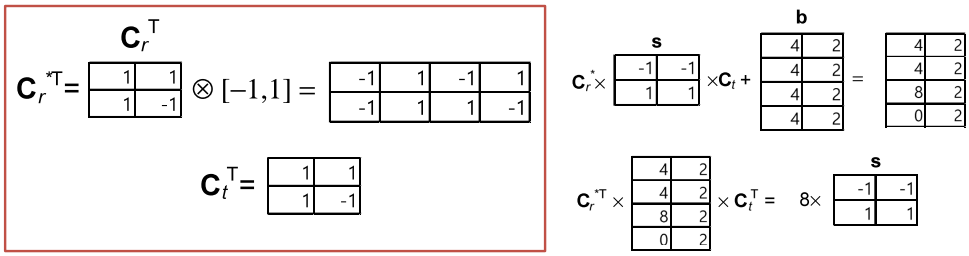

Fig. 3. Biased orthogonal matrix design by the Kronecker product with the Manchester code.

Let us consider OOK modulation of a Hadamard matrix with the conventional Manchester code. Every code 1 in $\boldsymbol{C}_t$ and $\boldsymbol{C}_r$ is replaced by $\{-1, 1\}$. Conversely, a code 0 is changed by $\{1, -1\}$. This will modulate the optical signal. Here, orthogonal properties are preserved so that $\boldsymbol{C}_t\boldsymbol{C}_t^{\top} = 2 \cdot N_{ct}$ and $\boldsymbol{C}_r^{\top}\boldsymbol{C}_r = 2 \cdot N_{cr}$. Let $\boldsymbol{C}_t^*$ and $\boldsymbol{C}_r^*$ be the expanded orthogonal matrices by replacing the individual codes with Manchester codes. Equations (7) and (8) are then expanded by using a Kronecker product $\otimes$ and its property for matrix multiplication

$$\begin{aligned}
\boldsymbol{C}_r^{*\top} \cdot \boldsymbol{J}_{2N_{cr},N_{ct}} &= \left(\boldsymbol{C}_r^{\top} \otimes \begin{bmatrix} -1 & 1 \end{bmatrix}\right) \cdot \boldsymbol{J}_{2N_{cr},N_{ct}} \\
&= \left(\boldsymbol{C}_r^{\top} \otimes \begin{bmatrix} -1 & 1 \end{bmatrix}\right) \cdot \left(\boldsymbol{J}_{N_{cr},N_{ct}} \otimes \begin{bmatrix} 1 \\ 1 \end{bmatrix}\right) \\
&= \left(\boldsymbol{C}_r^{\top} \cdot \boldsymbol{J}_{N_{cr},N_{ct}}\right) \otimes \left(\begin{bmatrix} -1 & 1 \end{bmatrix} \cdot \begin{bmatrix} 1 \\ 1 \end{bmatrix}\right) = 0 \qquad (9) \\
\boldsymbol{J}_{N_r,2N_t} \cdot \boldsymbol{C}_t^{*\top} &= \boldsymbol{J}_{N_r,2N_t} \cdot \left(\boldsymbol{C}_t^{\top} \otimes \begin{bmatrix} -1 \\ 1 \end{bmatrix}\right) \\
&= \left(\boldsymbol{J}_{N_r,N_t} \otimes \begin{bmatrix} 1 & 1 \end{bmatrix}\right) \cdot \left(\boldsymbol{C}_t^{\top} \otimes \begin{bmatrix} -1 \\ 1 \end{bmatrix}\right) \\
&= \left(\boldsymbol{J}_{N_r,N_t} \cdot \boldsymbol{C}_t^{\top}\right) \otimes \left(\begin{bmatrix} 1 & 1 \end{bmatrix} \cdot \begin{bmatrix} -1 \\ 1 \end{bmatrix}\right) = 0. \qquad (10)
\end{aligned}$$

Based on (9) and (10), consequently, any partial rows or columns in Hadamard matrices spread by Manchester code will satisfy (7) and (8). Fig. 3 shows another example of Manchester encoding and decoding in an order-2 Hadamard matrix. Compared to the former *W-H* matrix, the code length should be doubled to make perfect orthogonality between the matrix rows, but it is not necessary to remove the first row or the first column from the original matrix. Beyond 2*k*-order Hadamard matrices that are derived by the matrix with order two and successive Kronecker products, there is a conjecture that an $n \times n$ Hadamard matrix exists for $n = 1$ and $n = 2$, and $n = 4k$ for any $k \in N$ [15]. Since several construction techniques such as Paley, Williamson, and Baumert-Hall arrays have been developed, all 4*k*-orders of Hadamard matrices were found below 668 order. Moreover, an important property is that every Hadamard matrix can be transformed to a normalized Hadamard matrix where all entries in the first row and first column have the same order through a series of row or column permutations or inversion [20]. Without loss of generality, here, we summarize two construction methods for orthogonal codes in VLC MIMO from any Hadamard matrices with order-*n*.

(n-1 construction) In a normalized *n*-order Hadamard matrix $\boldsymbol{C}_n$ where $\boldsymbol{C}_n\boldsymbol{C}_n^{\top} = n\boldsymbol{I}_n$, $n = 2$ and $4k$ ($k \in N$), $\boldsymbol{C}_{n-1,n}$ is obtained by deleting the first row of $\boldsymbol{C}_n$. Then, $\boldsymbol{C}_{n-1,n}$ and $\boldsymbol{C}_{n-1,n}^{\top}$ can be used in $\boldsymbol{C}_t$ and $\boldsymbol{C}_r$.

(M construction) In an *n*-order Hadamard matrix $\boldsymbol{C}_n$, where $\boldsymbol{C}_n\boldsymbol{C}_n^{\top} = n\boldsymbol{I}_n$, $n = 1, 2$ and $4k$ ($k \in N$), $\boldsymbol{C}_{n,2n}^* = \boldsymbol{C}_n \otimes [\begin{smallmatrix} -1 \\ 1 \end{smallmatrix}]$ can be applied to $\boldsymbol{C}_r$. The maximum and minimum values of row sums in $\boldsymbol{C}_{n,2n}^*$ are equivalent to the ones in $\boldsymbol{C}_n$. Similarly, $\boldsymbol{C}_{2n,n}^* = \boldsymbol{C}_n \otimes \begin{bmatrix} -1 & 1 \end{bmatrix}$ can be applied to $\boldsymbol{C}_t$. The maximum and minimum values of column sums in $\boldsymbol{C}_{2n,n}^*$ are equivalent to the ones in $\boldsymbol{C}_n$.

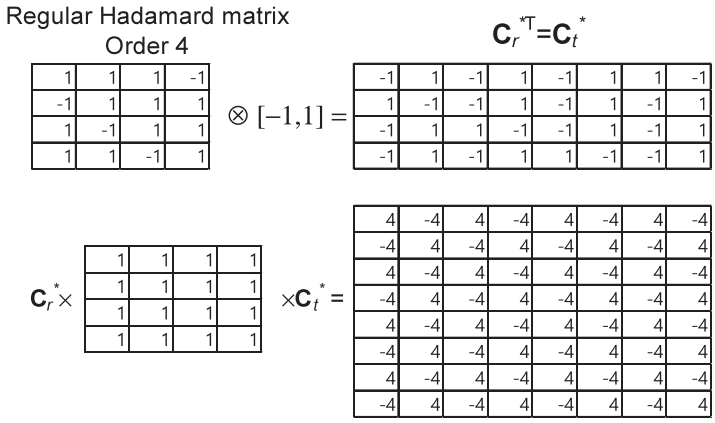

Fig. 4. Constant amplitude illumination by a regular Hadamard matrix.

Compared to *M construction* where an original signal is eventually modulated by $\{-1, 1\}$, *n-1 construction* consists of half-length codes and does not imply carrier modulation. However, ambient DC noises will also be removed by (7) and (8) in this case. Another useful feature for applying Hadamard matrices to VLC is that there can be no inherent flickers observed in the emitted code sequence, if the same message is broadcasting from emitters. A regular or a Bush-type Hadamard where row and column sums are constant can be utilized as $\boldsymbol{C}_n$ in minimizing flicker problems for *M constructions*. In the case of Bush-type Hadamard matrices, a $\boldsymbol{C}_n$ with $4k^2$-order, $2k$ column and row sums can be extracted [15], [20]. For example, a 16-order Bush-type Hadamard matrix has constant 4s in its row and column sums. Thus, if we transmit 1s or -1s in all elements of s with $\boldsymbol{C}_r$ and $\boldsymbol{C}_t$ of regular Hadamard matrices, all spread elements in $\boldsymbol{x}$ have the same values, accordingly. Setting proper values in $\boldsymbol{b}_t$ further helps the required brightness control. In this view, we can employ *M construction* to satisfy (7) or (8) derived from regular matrices. Column sums or row sums in *M construction* maintain the original absolute values of the column or row sums. It is clear that Kronecker products with element 1 or -1 do not change their absolute value of sums. Either copying or negation of the original value is conducted in this manner. Fig. 4 illustrates an example of the illumination of multiple drivers by using a 4×4 regular Hadamard matrix. Note that the full Hadamard matrix must be utilized in this case.

4. Experiments

In this section, we validate proposed matrices and the system model in an indoor positioning system by simulation and implementation results. we mainly focus on noise component $\boldsymbol{n}$ in (2), and show how it affects the positioning error. In the simulation, conventional trilateration is used to identify the location of indoor optical receivers by using the estimated distances from four LED sources to two receivers. The code rate of the simulation setup is chosen as 600 Hz. Four Hadamard matrices were used to construct $\boldsymbol{C}_t$. W-H with order 2 was employed as $\boldsymbol{C}_r$. Additionally, whole code sequence can be repeated until they fulfill different time requirements. Positions for LEDs and PDs and other model parameters are summarized in Table 1.

In Fig. 5(a), we first compare the distance errors expected among different Hadamard matrices according to the SNR after spread signal acquisition. The errors were calculated by the standard deviation for the estimated distances. The errors are mainly dependent on the code lengths that affect SNRs at the receivers based on (4). To reduce distance errors, successive signals can be accumulated at the receiver. Then the response time for a receiver should be increased accordingly. If independent random noise exists for every acquisition, the SNR for a de-spread signal increases by the square root of the number of accumulation times as in [15]. Fig. 5(b) shows the distance errors and the accumulated SNRs expected for the given response time. Response time is another

TABLE 1
Simulation Parameters

LED1	[0.50, 0.87, 1.95] m
LED2	[0.00, 0.00, 1.95] m
LED3	[1.00, 0.00, 1.95] m
PD1	[0.50, 0.29, 0.00] m
PD2	[0.50, 0.87, 0.00] m
$\Phi_{1/2}$, $\Psi_{1/2}$	30°
PD area (A)	9×10^{-6} m^2
LED carrier freq.	600 Hz
$\beta_{\mathbf{drv}}$	0.05 mC/chip
$\beta_{\mathbf{rcv}}$	1 chip/mC
$\alpha_{\mathbf{t}}$	0.19275 lm/mA
$\alpha_{\mathbf{r}}$	5.188 mA/lm

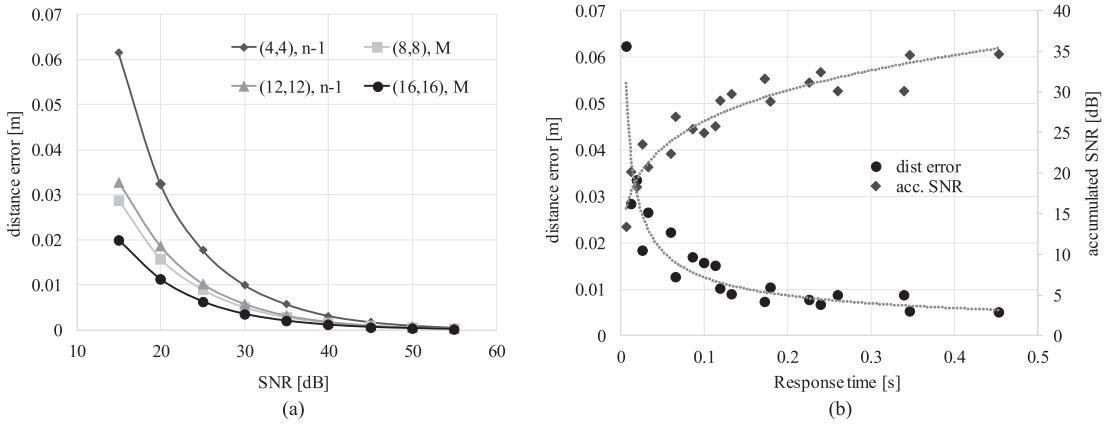

Fig. 5. Distance errors expected according to a change in the SNR. (a) Varying bit SNR. (b) Varying integration time.

important design metric for how fast the object movement can be observed at the detectors. To achieve less than 0.01 m standard error, more than 30 dB of total SNR is required in our simulation results. If we define it as the target SNR of the system, the corresponding response time in Fig. 5(b) is also required in conjunction with signal quality at the receiver. From the result, at least 100 ms of response time is needed to suppress the error below 0.01 m. To simultaneously ease the response time constraint and improve the SNR in (4), transmission energy E_s and PD area A should be increased. Generally, changing the specification, e.g., by increasing the transmission rates should consider the numerator term in (4) that results in dynamic position errors for given noise components.

We implemented three LED drivers and a receiver to test the feasibility as a positioning system in single carrier VLC. We could also validate the presented model and *M construction* of order-4 Hadamard matrix in these modules. In Fig. 6(a), the data flow of three emitters and a receiver is illustrated. One set of illuminators consists of a total of 9 white LEDs to increase effective area A for PD and all LED driving signals are controlled and synchronized by a microcontroller. Three sets of LED arrays were installed in the ceiling as shown in Fig. 6(b). There exist ambient light sources such as fluorescent light around lab. environments. A receiver module was movable on a flat table where the vertical distance to the LED arrays on the ceiling was 1.95 m. The carrier

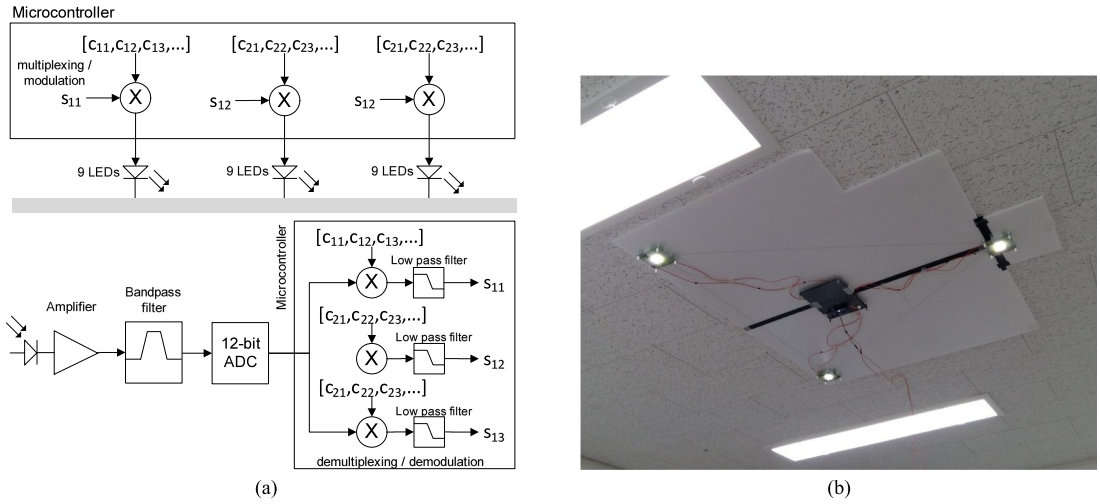

Fig. 6. Feasibility test setup for Hadamard matrix-based indoor positioning. (a) Signal processing flow. (b) Installation of three LED arrays on the ceiling.

frequency for the LEDs was selected as 600 Hz due to the limited responsibility of the commercial PD. Thus, the front-end circuitry of receivers has enough processing speed to detect the switching rate of the optical signals. Single code in *M construction* consists of only 1 chip of 600 Hz signal conforming to the response for pre-amplifier and filter stages. *M construction* by an order-4 W-H matrix was applied to $\boldsymbol{C}_t$, and $\boldsymbol{C}_r = 1$ for this setup. The main controller for the three light sources modulates and encodes the optical signals based on $\boldsymbol{s} \times \boldsymbol{C}_t$. The analog front-end circuit detects and amplifies the electrical signals sensed prior to digital conversion. Demodulation of the electrical signal is basically achieved by multiplication with $\boldsymbol{C}_r^\top$ and $\boldsymbol{C}_t^\top$ in (2), but further low pass filtering with 1 kHz cut-off frequency should be conducted to pick up only the DC components of interest. 10 over-sampled and digitized data for the 600 Hz receiving wave were de-modulated and further processed in digital low pass filter to obtain a fine DC component. Thus, frequencies of non-interest such as fluorescent light sources are eliminated by this process.

During the experiment, the receiver changes its location to 13 different pre-defined points including the center. These locations were defined as inside the triangular region formed by three LED arrays. The average SNR emitted from a LED source was measured as 34.8 dB at the receiver. After correcting the illumination differences among the LEDs, we obtained the location errors for the worst position according to the response time of the given system, as shown in Fig. 7(a). The errors were calculated by standard deviation of the distance samples to the ideal position. During the 13 ms. sensing time for the light sources, 0.02 m standard errors were observed. However, 0.009 m errors were estimated when the response time was increased to 100 ms. These dynamic errors mainly originate from the internal and external noise components, even if irregularity of the luminance pattern in a light source remains as static errors. Since dynamic behaviors on the observed optical signal at the fixed location appeared due to the noise components, we also plotted the observed SNRs for the decoded signals due to these noise factors in Fig. 7(b). Consequently, the implementation result agreed with the simulation result, with less than 4% mean error.

Table 2 shows results of the quantitative comparison results for several multiplexing techniques applicable to VLC positioning. While fixing E_s and σ, we set the maximum modulation frequency to 3 kHz for fair comparisons of different techniques. The number of carriers, required sensing time and the standard deviation of positions errors are also listed for the comparison. As demonstrated by the results, two techniques in this paper efficiently suppress the standard errors for positioning, while the required sensing time and the number of carriers can be reduced more than the existing techniques. This was induced by the fact that our construction gives not only reduced sensing time

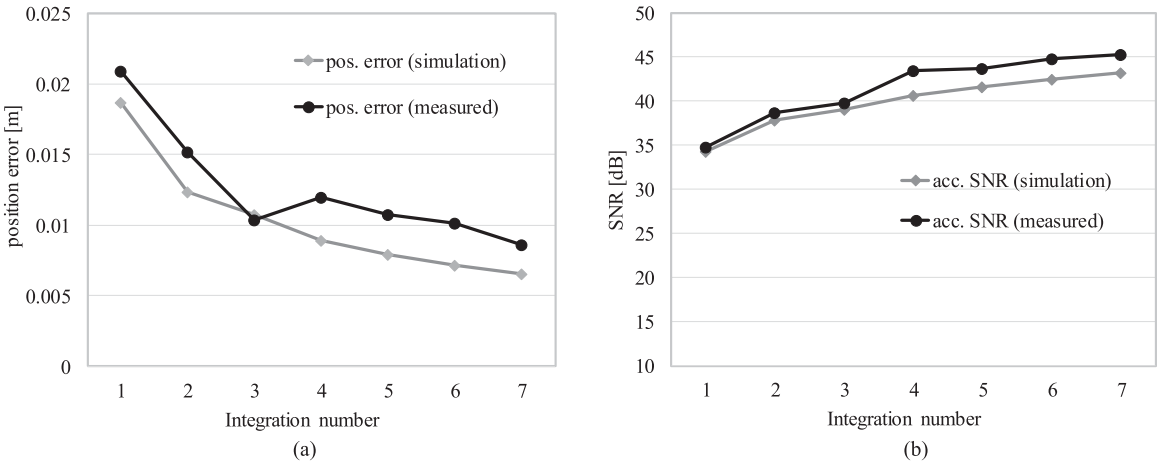

Fig. 7. Location errors and SNRs observed according to integration time. (a) Location errors. (b) Observed SNRs after decoding.

TABLE 2
Comparisons for Multiplexing Techniques at 2.03 m Distance From Three Sources Where $E_s = 510\ \mu J$ and $\sigma = 6.09 \times 10^{-7}$

Multiplexing techniques	Time-multiplexed [21]	Orthogonal frequency [24]	CDMA: BIBD(7,3,1) [22], [23]	CDMA: random optical code* [11], [13]	CDMA: This work (*n-1*)	CDMA: This work (*M*)
Modulation freq. [kHz]	3	1, 2 and 3	3	3	3	3
# of carriers	1	3	1	1	1	1
Min. sensing time required [ms]	5.0	13.3	11.7	13.3	6.7	13.3
std. error [m]	0.48	0.07	0.07	0.27	0.12	0.01

*two random pulses over 8 spread code were chosen.

required for multiplexing with a variety of orders and but also shows perfect orthogonality between different transmitting codes.

5. Conclusions

This paper presents the Hadamard matrix design for a single or a no carrier VLC positioning system. To provide non-negative signaling and orthogonality in VLC, orthogonal matrices can be created by both *n−1* and *M construction* derived from the existing 2 and 4*k* Hadamard matrices with proper bias control. The variety of orders in Hadamard matrices and their variants can help conform to numerous specifications for VLC MIMO including the number of concurrent transmitters, receivers and user response time. The structure presented in this paper can also be extended to the use of orthogonal frequencies where the orthogonality is still represented by the full or partial form of the Hadamard matrices.

References

[1] Y. U. Lee and M. Kavehrad, "Two hybrid positioning system design techniques with lighting LEDs and ad-hoc wireless network," *IEEE Trans. Consum. Electron.*, vol. 58, no. 4, pp. 1176–1184, Nov. 2012.

[2] I.-C. Lu, C. H. Yeh, D.-Z. Hsu, and C.-W. Chow, "Utilization of 1-GHz VCSEL for 11.1-Gbps OFDM VLC wireless communication," *IEEE Photon. J.*, vol. 8, no. 3, Jun. 2016, Art. no. 7904106.

[3] A. T. Hussein and J. M. H. Elmirghani, "Mobile multi-gigabit visible light communication system in realistic indoor environment," *J. Lightw. Technol.*, vol. 33, no. 15, pp. 3293–3307, Aug. 2015.

[4] T. Faith and H. Haas, "Performance comparison of MIMO techniques for optical wireless communications in indoor environments," *IEEE Trans. Commun.*, vol. 61, no. 2, pp. 733–742, Feb. 2013.

[5] Q. Wang, Z. Wang, and L. Dai, "Multiuser MIMO-OFDM for visible light communications," *IEEE Photon. J.*, vol. 7, no. 6, Dec. 2015, Art. no. 7904911.

[6] T.-H. Do and M. Yoo, "An in-depth survey of visible light communication based positioning systems," *Sensors*, vol. 16, no. 5, May 2016, Art. no. 678.

[7] L. Zeng *et al.*, "High data rate multiple input multiple output (MIMO) optical wireless communications using white LED lighting," *IEEE J. Sel. Areas Commun.*, vol. 27, no. 9, pp. 1654–1662, Dec. 2009.

[8] S. D. Dissanayke and J. Armstrong, "Comparison of ACO-OFDM, DCO-OFDM and ADO-OFDM in IM/DD systems," *J. Lightw. Technol.*, vol. 31, no. 7, pp. 1063–1072, Apr. 2013.

[9] D. J. F. Barros, S. K. Wilson, and J. M. Kahn, "Comparison of orthogonal frequency-division multiplexing and pulse-amplitude modulation in indoor optical wireless links," *IEEE Trans. Commun.*, vol. 60, no. 1, pp. 153–163, Jan. 2012.

[10] R. Mesleh, H. Elgala, and H. Haas, "On the performance of different OFDM based optical wireless communication systems," *J. Opt. Commun. Netw.*, vol. 3, no. 8, pp. 620–628, Aug. 2011.

[11] M. F. Guerra-Medina, B. Rojas-Guillama, O. Gonzalez, J. A. Martin-Gonzalez, E. Poves, and F. J. Lopez-Hernandez, "Experimental optical code-division multiple access system for visible light communications," in *Proc. Wireless Telecommun. Symp.*, Apr. 2011, pp. 1–6.

[12] P. H. Pathak, X. Feng, P. Hu, and P. Mohapatra, "Visible light communication, networking and sensing: A survey, potential and challenges," *IEEE Comm. Surveys Tuts.*, vol. 17, no. 4, pp. 2047–2076, Sep. 2015.

[13] M. F. Guerra-Medina, O. Gonzalez, B. Rojas-Guillama, J. A. Martin-Gonzalez, F. Delgado, and J. Rabadan, "Ethernet-OCDMA system for multi-user visible light communications," *Electron. Lett.*, vol. 8, no. 4, pp. 227–228, Feb. 2012.

[14] Y.-A. Chen, Y.-T. Chang, Y.-C. Tseng, and W.-T. Chen, "A framework for simultaneous message broadcasting using CDMA-based visible light communications," *IEEE Sens. J.*, vol. 15, no. 12, pp. 6819–6827, Dec. 2015.

[15] J. K. Park, C.-J. Lee, D.-Y. Kim, J.-H. Chun, and J. T. Kim, "Application of weighing matrices to simultaneous driving technique for capacitive touch sensors," *IEEE Trans. Consum. Electron.*, vol. 61, no. 2, pp. 261–269, May 2015.

[16] S. Rajagopal, R. D. Roberts, and S.-K. Lim, "IEEE 802.15.7 visible light communication: Modulation schemes and dimming support," *IEEE Commun. Mag.*, Mar. 2012, pp. 72–82.

[17] J. M. Kahn and J. R. Barry, "Wireless infrared communications," *Proc. IEEE*, vol. 85, no. 2, pp. 265–298, Feb. 1997.

[18] K. Cui, G. Chen, Z. Xu, and R. D. Roberts, "Line-of-sight visible light communication system design and demonstration," in *Proc. 7th Int. Conf. Comm. Syst. Netw. Digit. Signal Process.*, Jul. 2010, pp. 621–625.

[19] L.-G. Alberto, "Chapter 5 sums of random variables and long-term averages," in *Probability and Random Processes for Electrical Engineering*, 2nd ed. Reading, MA, USA: Addison-Wesley, May 1994, pp. 270–272.

[20] C. J. Colbourn and J. H. Dinitz, *Handbook of Combinatorial Designs*, 2nd ed. Boca Raton, FL, USA: CRC, 2006.

[21] W. Zhang, M. I. S. Chowdhury, and M. Kavehrad, "Asynchronous indoor positioning system based on visible light communications," *J. Opt. Eng.*, vol. 53, no. 4, Apr. 2014, Art. no. 045105.

[22] N. Mohammad and B.-P. Maite, "Application of expurgated PPM to indoor visible light communications," *J. Lightw. Technol.*, vol. 32, no. 5, pp. 875–882, Mar. 2014.

[23] F. R. K. Chung, J. A. Salehi, and V. H. Wei, "Optical orthogonal codes: Design, analysis and applications," *IEEE Trans. Inf. Theory*, vol. 35, no. 3, pp. 595–604, May 1989.

[24] H.-S. Kim, D.-R. Kim, S.-H. Yang, Y.-H. Son, and S.-K. Han, "An indoor visible light communication positioning system using a RF carrier allocation technique," *J. Lightw. Technol.*, vol. 31, no. 15, pp. 134–144, Jan. 2013.